



HAL
open science

Revisiting the paleomagnetism of Muong Nong layered tektites: Implications for their formation process

J. Gattacceca, Pierre Rochette, Yoann Quesnel, Sounthone Singsoupho

► To cite this version:

J. Gattacceca, Pierre Rochette, Yoann Quesnel, Sounthone Singsoupho. Revisiting the paleomagnetism of Muong Nong layered tektites: Implications for their formation process. *Meteoritics and Planetary Science*, 2021, 10.1111/maps.13703 . hal-03283291

HAL Id: hal-03283291

<https://hal.science/hal-03283291v1>

Submitted on 22 Oct 2021

HAL is a multi-disciplinary open access archive for the deposit and dissemination of scientific research documents, whether they are published or not. The documents may come from teaching and research institutions in France or abroad, or from public or private research centers.

L'archive ouverte pluridisciplinaire **HAL**, est destinée au dépôt et à la diffusion de documents scientifiques de niveau recherche, publiés ou non, émanant des établissements d'enseignement et de recherche français ou étrangers, des laboratoires publics ou privés.

METEORITICS & PLANETARY SCIENCE

**Revisiting the paleomagnetism of Muong Nong layered
tektites: implications for their formation process**

Journal:	<i>Meteoritics & Planetary Science</i>
Manuscript ID	MAPS-3583
Manuscript Type:	Article
Date Submitted by the Author:	20-Apr-2021
Complete List of Authors:	Gattacceca, Jérôme; CEREGE, Rochette, Pierre; Aix Marseille University CNRS, CEREGE Quesnel, Yoann; Aix-Marseille University, CEREGE Singsoupho, Sounthone; National University of Laos, Department of Physics, Faculty of Natural Sciences
Keywords:	Muong Nong tektite, magnetic properties, Paleomagnetism, Australasian < Tektite(s)

SCHOLARONE™
Manuscripts

1
2
3 1 **Revisiting the paleomagnetism of Muong Nong layered tektites: implications for their**
4
5 2 **formation process**
6
7
8 3
9

10 4 Jérôme Gattacceca¹, Pierre Rochette¹, Yoann Quesnel¹, Sounthone Singsoupho²

11 5 ¹CNRS, Aix-Marseille Univ, IRD, INRAE, Aix-en-Provence, France

12 6 ²Department of Physics, Faculty of Natural Sciences, National University of Laos, Vientiane,
13
14
15
16
17 7 Laos
18

19 8

20
21 9 **Abstract**
22

23
24 10 Among Australasian tektites, the so-called Muong Nong tektites stand out for their peculiar
25
26 11 layering and blocky aspect. Although the source crater for the Australasian tektites is not
27
28 12 known, Muong Nong tektites are generally considered as a relatively proximal ejecta. The
29
30 13 mechanism responsible for the formation of the layering has been a matter of debate. In this
31
32 14 work, we revisit the paleomagnetism of Muong Nong tektites. They retain a thermoremanent
33
34 15 magnetization acquired during cooling below 585°C in the presence of the ambient
35
36 16 geomagnetic field, and carried magnetite in most samples, although at least one sample
37
38 17 containing metallic iron was detected. The inclination of the paleomagnetic direction with
39
40 18 respect to the layering plane clusters around $18 \pm 12^\circ$, compatible with the inclination of the
41
42 19 geomagnetic field for this latitude at the time of impact. This indicates that the layering of the
43
44 20 Muong Nong tektites was sub-horizontal while they were cooling below 585°C. The preferred
45
46 21 scenario for the formation of the layering of layered tektite is therefore by horizontal shear in
47
48 22 pools or sheets of molten material.
49
50
51
52
53
54 23
55
56
57
58
59
60

24

25 1. Introduction

26 Tektites are glassy bodies formed by high-temperature melting of target rocks during
27 hypervelocity impacts at the surface of the Earth, and spread over extensive strewnfields (Glass,
28 1990). Five tektite fields are known: Australasian tektites, belizites, moldavites, ivoirites,
29 North-American tektites, by order of increasing age (Koeberl, 1994; Rochette et al., 2021). All
30 can be associated to a known impact crater, except Australasian tektites whose source is yet not
31 firmly identified, although it has been recently proposed to be hidden under a volcanic plateau
32 in Southern Laos (Sieh et al., 2020). This is surprising in view of their relatively young age of
33 788 ± 3 ka (Jourdan et al., 2019), the assumed large diameter of the putative crater and extensive
34 spread over at least 180 million km^2 (28% of the surface of the Earth) when including
35 microtektites found in deep sea sediments and Antarctica (Folco et al., 2008; Di Vincenzo al.,
36 2021). A source crater located in Indochina is favored by most authors based on tektite and
37 microtektite distribution (Glass and Pizzuto, 1994; Glass and Koeberl, 2006), despite
38 alternative locations proposed in Northern China (Mizera et al., 2016). However, such a crater
39 has not been confirmed so far. In the absence of crater, competing hypotheses of formation by
40 multiple km-sized craters (Wasson, 1991), or airburst without the need for an impact crater
41 have emerged for the Australasian tektites (e.g., Barnes, 1963; Wasson, 2003). Besides the
42 Australasian tektite case, this debate has far-reaching implications for the understanding of the
43 possible risk and environmental effects associated with large airbursts (e.g., Cavosie and
44 Koeberl, 2019).

45 Of particular interest in this debate are the Muong-Nong tektites, a sub-category of Australasian
46 tektites characterized by their larger size (up to above 20 kg), blocky aspect without the typical
47 splashforms attesting solidification during flight, and marked layering with adjacent dark and
48 light layers showing differences in chemical composition (Koeberl, 1992). These objects, also

1
2
3 49 called simply “layered tektites” were named after the town in Laos where they were first
4
5 50 identified (Lacroix, 1935). They are found in abundance over an area of ~1000 km radius in
6
7 51 East Thailand, South Central Vietnam and Laos (e.g., Barnes, 1971; Koeberl, 1992; Fiske et
8
9 52 al., 1999; Schnetzler, 1992; Schnetzler and Mc Hone, 1996; Wasson et al. 1995; Fiske et al.
10
11 53 1999). Layering was proposed to be formed by differential flow of melt with different
12
13 54 viscosities in a melt sheet, melt pools or melt puddles along gently inclined surfaces (e.g.,
14
15 55 Barnes and Pitakpaivan, 1962; Barnes, 1963; Wasson et al., 2003). Geochemistry favors a
16
17 56 formation from an ejected inhomogeneous melt flowing after reaching the surface (e.g.,
18
19 57 Koeberl, 1992). But other models, such as stretching in flight and/or deformation during landing
20
21 58 of large masses of molten material have been proposed (Fiske, 1996). Muong Nong tektites are
22
23 59 also characterized, with respect to standard splashform australasites, by 1) a higher volatile
24
25 60 content (water, noble gases, etc., see Beran and Koeberl 1997; Koeberl, 1992; Mizote et al.,
26
27 61 2003), 2) pressure of gas bubbles within the atmospheric range, while splashforms bubble
28
29 62 pressure estimates suggests solidification outside the atmosphere (Mizote et al., 2003; Žák et
30
31 63 al., 2019), 3) preservation of crystalline inclusions of coesite, cristobalite, zircon, magnetite
32
33 64 (Glass and Barlow, 1979; Kleinman, 1969; Krizova et al., 2019; Cavosie et al., 2018; Masotta
34
35 65 et al. 2020) indicative of lower peak temperatures.
36
37
38
39
40
41
42

43 66 Models of layering formation by flow in a melt pool or melt sheet (formed either by fallout of
44
45 67 liquid ejecta from an impact, or by in situ melting by an airburst) all require that the layering of
46
47 68 Muong Nong tektites was sub horizontal during cooling in the Earth magnetic field. Therefore,
48
49 69 the angle between layering and natural remanent magnetization (NRM), should be close to the
50
51 70 expected inclination of the geomagnetic field at that time, i.e. 28° for a site at latitude 15°N. In
52
53 71 this work, following the pioneering study of de Gasparis et al. (1975), we revisited Muong-
54
55 72 Nong tektite paleomagnetism to bring further constraints to their original position at the surface
56
57 73 during cooling. Indeed, the work by de Gasparis (1973) and de Gasparis et al. (1975) was
58
59
60

1
2
3 74 focused primarily on the paleointensity of the magnetic field recorded by the tektites, with the
4
5 75 objective of determining if tektites were of lunar or terrestrial origin, an active debate at that
6
7 76 time. The directional data were only briefly mentioned and discussed, and it was John Wasson
8
9 77 who wrote “*I suggest that the remanence should be measured again...*” (Wasson, 2003), and
10
11 78 initiated this second study of Muong Nong tektites paleomagnetism.
12
13
14
15
16
17

18 80 **2. Samples**

19
20
21 81 Tektites are usually characterized by a purely paramagnetic behavior (Rochette et al. 2015,
22
23 82 2019), not adapted for paleomagnetic investigations that require at least 10 ppm of
24
25 83 ferromagnetic inclusions such as magnetite or metal. However, it appears that Muong Nong
26
27 84 tektites contain a significant amount of such inclusions (Kleinman et al., 1969; Glass and
28
29 85 Barlow, 1979; Rochette et al., 2015), making them suitable for a paleomagnetic study (de
30
31 86 Gasparis et al., 1975).
32
33
34

35 87 We studied 32 samples taken from 18 Muong Nong tektites (Table 1, Figure 1). They were
36
37 88 selected for their marked layering (Figure 2). Nine tektites, with label starting with T or TS
38
39 89 were selected and characterized by John Wasson. Seven tektites, with label starting with N,
40
41 90 were recovered and selected by Pierre Rochette within five collection sites prospected during a
42
43 91 field trip in 2019 around the Muong Nong locality in Southern Laos. The larger samples were
44
45 92 bought directly from villagers who collected them while cultivating their fields, thus ensuring
46
47 93 that the coordinates given in Table 1 are reliable. Finally, two samples (MNP1, MNP2) were
48
49 94 obtained from a dealer in Thailand. Selection criteria were well-expressed planar unfolded
50
51 95 layering (apart from sample N16, see below), large enough size to allow cutting samples of a
52
53 96 few cm³ lacking magnetic soil incrustations that often found in the porous parts of Muong Nong
54
55 97 tektites. We encountered a significant number of Muong Nong where folding of layering
56
57 98 prevented the definition of a consistent presumed paleo-horizontal plane for the whole tektite.
58
59
60

1
2
3 99 To document the paleomagnetic signal behavior of such samples, we cut one folded sample
4
5 100 (tektite N16) perpendicular to the fold axis, obtaining four subsamples, two from the fold flanks
6
7 101 with a $\sim 40^\circ$ angular difference, and two from the fold hinge.
8
9

10 102 Field observations consistently show that Muong Nong tektites, when found *in situ*, occur near
11
12 103 the contact between the upper yellow sandy soil formation and an underlying more consolidated
13
14 104 red formation rich in lateritic gravel (Schneztler and McHone, 1996; Wasson et al., 1995; Tada
15
16 105 et al., 2020; Zak et al. 2019, and our own field work in 2019). Previous interpretations in terms
17
18 106 of subsequent deposition of the soil (called loess-like or “catastro-loess” by some authors, see
19
20 107 review in Mizera et al., 2016) on top of a lateritic surface on which the Muong Nong tektite fell
21
22 108 or formed by in situ melting may be too simplistic. In fact, the “loess-like” material is typical
23
24 109 of poor podzolic soils commonly found in hilly zones of tropical humid areas. Between this soil
25
26 110 and the lateritic formation, a stone line (rich in quartz pebbles) is consistently observed. Stone
27
28 111 lines are usually interpreted as accumulation of insoluble matter after pedogenetic dissolution.
29
30 112 Therefore, the in situ position of tektites may not reflect their deposition position but long term
31
32 113 pedogenetic processes. Our prospection around Muong Nong locality showed that most sites
33
34 114 producing Muong Nong tektite were lateritic gravels pits dug to provide material for dirt roads.
35
36 115 Those pits allowed to clearly observe that the Muong Nong tektites, when recovered in situ,
37
38 116 have their layering often but not always presently horizontal, and do not occur as a continuous
39
40 117 thin layer. The largest continuous layer we observed (with a maximum thickness of 4 cm) was
41
42 118 followed along less than one meter laterally. The largest samples we recovered in situ and
43
44 119 bought were 150 and 458 g, respectively.
45
46
47
48
49
50
51

52 120

53 54 55 121 **3. Methods**

56
57
58 122 After initial measurement of their bulk natural remanent magnetization (NRM), samples were
59
60 123 cut into mutually-oriented subsamples using a wire saw cooled with water. Sample size was

1
2
3 124 chosen based on the initial NRM measurement to aim for a NRM of at least 10^{-6} Am² allowing
4
5 125 reliable remanence measurements. Cutting was also aimed at removing the external, weathered
6
7 126 part of the tektites, with particular attention to soil incrustations that may be highly magnetic
8
9 127 compared to the bulk tektite glass. Additional cleaning was performed using a non magnetic
10
11 128 metallic needle, and for some samples with an additional treatment with ethanolamine
12
13 129 thioglycolate (EATG) to dissolve remaining adhering terrestrial oxihydroxides. An oriented
14
15 130 thin slice was cut from most sample to better define the layering (Figure 2).

16
17
18
19 131 Magnetic measurements were performed at CEREGE. The magnetic susceptibility was
20
21 132 measured using a MFK1 kappabridge from Agico. Hysteresis properties were measured with a
22
23 133 Princeton Micromag vibrating sample magnetometer with a maximum applied field of 1T and
24
25 134 a moment sensitivity of $\sim 10^{-8}$ Am². Magnetic remanence was measured with a SQUID
26
27 135 magnetometer (2G Enterprises, model 755R, with noise level of 10^{-11} Am²), except for the
28
29 136 initial NRM of large bulk specimens that was measured with a spinner magnetometer (Minispin
30
31 137 model from Molspin). Stepwise alternating field (AF) and thermal demagnetization were used
32
33 138 to characterize the NRM. AF demagnetization was performed using the in-line three-axis
34
35 139 demagnetization of the 2G magnetometer, or off-line by three-axis demagnetization with a
36
37 140 LDA5 AF demagnetizer from Agico. Thermal demagnetization was performed with a zero-
38
39 141 field oven from ASC. Saturation isothermal remanent magnetization (sIRM) was imparted in a
40
41 142 field of 3 T with MMPM9 pulse magnetizer. Anhysteretic remanent magnetization was
42
43 143 imparted using the LDA5AF instrument. Magnetization components were computed from
44
45 144 NRM demagnetization data by principal component analysis (Kirschvink, 1980), using the
46
47 145 Paleomac software (Cogné, 2003).

54
55 146

57 147 **4. Intrinsic magnetic properties**

58
59
60

1
2
3 148 The intrinsic magnetic properties of the 18 studied Muong Nong tektites, shown in Table 2, can
4
5 149 be compared to previous results for Australasian tektites that are mostly paramagnetic with only
6
7 150 traces of ferromagnetic inclusions below 1 ppm (see review in Rochette et al., 2015). The
8
9 151 average susceptibility for the studied Muong Nong tektites ($94.1 \pm 17.4 \times 10^{-9} \text{ m}^3/\text{kg}$, $n=18$) is
10
11 152 higher than the average for Australasian tektites of $82 \pm 10 \times 10^{-9} \text{ m}^3/\text{kg}$, $n=152$ (Rochette et al.,
12
13 153 2015). Similarly, the average saturation remanence (sIRM) of our sample set is $5.20 \pm 3.30 \times 10^{-5}$
14
15 154 Am^2/kg , higher than what is observed in the general Australasian tektite population ($\leq 4 \times 10^{-6}$
16
17 155 Am^2/kg in Rochette et al., 2015).

18
19
20
21
22 156 Hysteresis properties were measured for subsamples of the six tektites with magnetic
23
24 157 susceptibility significantly higher than the average value of $94.1 \times 10^{-9} \text{ m}^3/\text{kg}$. All cycles
25
26 158 (corrected for the high-field susceptibility computed over the interval 0.8-1 T) are typical of
27
28 159 pseudo-single domain magnetite, with the exception of sample T428 that has a hysteresis loop
29
30 160 with low B_C , high B_{CR}/B_C and curvature up to 0.7 T (Figure 3A), typical of the presence of
31
32 161 multidomain metallic iron as observed in iron metal-bearing meteorites (e.g., Gattacceca et al.,
33
34 162 2014). The saturation magnetization (M_S) in magnetite-bearing samples ranges from 8.0×10^{-4}
35
36 163 to $1.66 \times 10^{-2} \text{ Am}^2/\text{kg}$, indicating a magnetite content in the 8.7 ppm to 180 ppm range. The ratios
37
38 164 M_{RS}/M_S and B_{CR}/B_C indicate that the magnetite grains are in the pseudo-single domain state
39
40 165 (Dunlop, 2002), i.e. in the 80-200 nm size range for equant grains (Muxworthy and Williams,
41
42 166 2015). The M_S value of sample T428 suggests the presence of 58 ppm of metallic iron whose
43
44 167 multidomain behavior indicates a grain size above 100 nm. There is no indication of the
45
46 168 presence of superparamagnetic grains (Figure 3B).

47
48
49
50
51
52
53 169 Thermal demagnetization of the NRM shows a sharp decrease in magnetization at temperatures
54
55 170 in the 570-580°C range (Figure 4A), suggesting that the main remanence carrying mineral is
56
57 171 magnetite that has a Curie temperature of 585°C. Sample T428, whose main magnetic carrier
58
59 172 is metal was not demagnetized thermally by lack of available material.

1
2
3 173 Demagnetization of sIRM by AF (Figure 4B) shows coercivity spectra in agreement with
4
5 174 pseudo-single domain magnetite, with median destructive fields of 21 ± 8 mT. The median
6
7 175 destructive field of ARM is 31 ± 9 mT. After AF demagnetization of 100 mT, less than 10% of
8
9 176 the sIRM is left in 14 out of 17 tektites (Table 1). Only 3 samples stand out with higher residual
10
11 177 IRM after AF demagnetization of 100 mT: T428 (24 %) whose hysteresis properties suggest
12
13 178 that it contains metal instead of magnetite, T490 (23%), and N19 (18%). We have no hysteresis
14
15 179 data for T490 and N19, but a sample of T490 was demagnetized thermally and shows a
16
17 180 unblocking temperature spectrum that is different from the other tektites, with a marked
18
19 181 decrease of NRM starting at 490°C rather than 560°C (Figure 4A). This may evidence the
20
21 182 presence of metal that is being destroyed rather than demagnetized during the thermal
22
23 183 treatment.
24
25
26
27
28
29 184

30 31 185 **5. Paleomagnetism**

32
33
34 186 All paleomagnetic results are summarized in Table 3.

35 36 37 187 *5.1. Tektites affected by lightning-generated magnetic fields*

38
39
40 188 The NRM intensities span 4 orders of magnitude, ranging from 10^{-7} to 10^{-3} Am²/kg. This is in
41
42 189 contrast with the more restricted range of 10^{-7} to 10^{-5} Am²/kg obtained by de Gasparis et al.
43
44 190 (1975). NRM/sIRM ratios of the ten samples with highest NRM are close to, or exceeds 0.1,
45
46 191 suggesting that these tektites were exposed to a strong field at some point in their history. This
47
48 192 is confirmed by the more refined comparison of AF demagnetization data of NRM and sIRM
49
50 193 (Figure 5), using the so-called REM' approach (Verrier and Rochette, 2002; Gattacceca and
51
52 194 Rochette, 2004). While most samples have REM' values below 0.1, five samples with strong
53
54 195 NRM/sIRM have REM' values well above 0.1 over the whole upper range of their coercivity
55
56 196 spectrum (samples N03A, N03B, N17, N20A, T419). It is noteworthy that the REM' values of
57
58
59
60

1
2
3 197 these samples are below 0.1 for AF fields below 5-10 mT, evidencing relaxation of their strong
4
5 198 field magnetization over time.
6
7

8 199 The orthogonal projection plots of AF and thermal demagnetization data for sample N17 are
9
10 200 shown in Figure 6. The other samples with strong NRM and strong REM' show an identical
11
12 201 behavior and are not shown. The orthogonal plot for the AF demagnetization data does not
13
14 202 show the curvature typical of exposure to hand magnets, a bad habit that is deeply encroached
15
16 203 in the meteorite hunters and collectors (see e.g., Gattacceca et al., 2014). Moreover, the REM'
17
18 204 values above 0.1 extends up to 100 mT, setting a lower limit for the strong field responsible for
19
20 205 the magnetization (Verrier and Rochette, 2002). In view of the original sample size (above 36
21
22 206 g and up to 275 g), such strong and large magnetic fields if artificial, would only be generated
23
24 207 by very large rare earth magnets or electromagnets, not available on the field. Therefore,
25
26 208 remagnetization by an artificial magnetic field seems highly improbable. The best explanation
27
28 209 to account for their strong NRM is remagnetization by lightning strikes. Such phenomenon is
29
30 210 well-known in paleomagnetic studies and result in demagnetization diagrams and NRM/sIRM
31
32 211 ratios similar to what we observed here (e.g., Verrier and Rochette, 2002). For samples that
33
34 212 have been at the surface or subsurface for ~ 0.8 Myr in a tropical climatic setting, such
35
36 213 remagnetization can indeed be expected. Lightning may have occurred any time between the
37
38 214 present and 0.8 Ma, thus accounting for the viscous decay of the lower coercivity IRM. These
39
40 215 samples cannot be used for the main purpose of our work that require preservation of the
41
42 216 original magnetization of the tektites.
43
44
45
46
47
48
49

50 217 Two samples, MNP1 and N20B, have high NRM/sIRM ratio (6.01×10^{-2} and 1.14×10^{-1}) and
51
52 218 two components of magnetization (Figure 6). But high REM' > 0.1 are restricted to the lower
53
54 219 coercivity component in these two samples: although the low coercivity component was
55
56 220 acquired in a strong magnetic field of ~ 20 -40 mT, the high coercivity component is not a strong
57
58 221 field magnetization and is discussed further.
59
60

1
2
3 222
4
5
6 223

5.2. Tektite with folded layering

7
8
9 224 The four subsamples originating from the tektite sample that was selected for its folded layering
10
11 225 (N16) were thermally demagnetized. They all provided a medium temperature (MT) component
12
13 226 isolated between $\sim 180^{\circ}\text{C}$ and $\sim 550^{\circ}\text{C}$, and a high temperature component (HT) isolated
14
15 227 between $\sim 550^{\circ}\text{C}$ and 580°C (Figure 6). Both components do not pass a fold test at the 95%
16
17 228 confidence level (McElhinny, 1964). We also tested stepwise unfolding of the four direction,
18
19 229 and the maximum grouping is obtained for zero unfolding. This means that the magnetization
20
21 230 was acquired after the layering was in its present folded state. The MT (resp. HT) directions are
22
23 231 similar for the four sub-samples, with a Fisher precision parameter of 35 (resp. 69). The mean
24
25 232 MT and HT directions differ by 22.5° and are distinct at the 99% confidence level using the
26
27 233 statistical test of McFadden and McElhinny (1990). The negative fold test indicates that folding
28
29 234 of the layering occurred at temperature higher than 585°C , in agreement with a glass transition
30
31 235 temperature of about 700°C in tektites indicating that the glass ceases to be plastic below this
32
33 236 temperature (Arnd and Rombach, 1976; Wilding et al. 1996).

34
35
36
37
38
39 237
40
41

5.3. Tektites with planar layering

42 238
43
44 239 Discarding the six tektites (10 sub-samples) that were affected by lighting-induced magnetic
45
46 240 fields, the average NRM is $1.52 \times 10^{-6} \text{ Am}^2/\text{kg}$, and the median NRM is $7.48 \times 10^{-7} \text{ Am}^2/\text{kg}$ ($n=23$
47
48 241 samples). The observed range (5×10^{-8} to $4 \times 10^{-6} \text{ Am}^2/\text{kg}$) agrees with the observations of de
49
50 242 Gasparis et al. (1975). The demagnetization data are presented in Figure 6. Origin-trending
51
52 243 high-temperature (HT) and high coercivity (HC) components could be isolated in all samples.
53
54 244 All samples have relatively well-defined paleomagnetic directions with an average maximum
55
56 245 angular deviation (MAD, as defined by Kirschvink, 1980) of $9.8 \pm 6.3^{\circ}$. The HT component is
57
58
59
60

1
2
3 246 unblocked up to 580°C (Figure 4A). The HC component is unblocked up to alternating fields
4
5 247 between 50 mT and above 100 mT (Figure 4C), depending on the coercivity spectrum of the
6
7 248 samples (Figure 4B). These components are similar in direction among mutually oriented
8
9
10 249 samples of the same tektite. The average angular difference between HT and HC components
11
12 250 for mutually oriented samples is 15°, which can be attributed to orientation uncertainties and to
13
14 251 the uncertainties on the direction of the magnetization components themselves as reflected by
15
16 252 their MAD. The HT/HC components are therefore considered as characteristic remanent
17
18 253 magnetizations (ChRM). The paleomagnetic declination is meaningless because samples were
19
20 254 recovered as loose non oriented blocks. Therefore, only the absolute value of the inclination,
21
22 255 computed with respect to the petrographic layering plane, has a meaning and is given in Table
23
24 256 3. A number of tektites also display a medium temperature (MT), medium coercivity (MC)
25
26 257 component of magnetization. The MT components are typically unblocked up 540-560°C,
27
28 258 while the MC components are unblocked up to 15-20 mT (Figure 6).
29
30
31
32
33 259 During thermal demagnetization, the NRM is unblocked up to the Curie temperature of pure
34
35 260 magnetite (Figure 4A), except for sample T490 whose NRM is fully unblocked at 570°C, but
36
37 261 as discussed above, this sample may have metal instead of magnetite as magnetic carrier. This
38
39 262 indicates that the magnetization is likely of thermoremanent origin, and was acquired upon
40
41 263 cooling from a temperature above 585°C. The REM' ratios, integrated over the HC component,
42
43 264 are in the range of $\sim 2 \cdot 10^{-2}$ typical of a thermoremanence in the geomagnetic field (Gattacceca
44
45 265 and Rochette, 2004). Therefore, these tektites were magnetized while in a fixed position with
46
47 266 respect to the ambient magnetic field. In particular, this precludes that the samples were in flight
48
49 267 (spinning) while they were cooling below 585°C. This cooling phase must have taken place
50
51 268 with the tektites in a fixed position on the ground at least between 585°C and 100-200°C (the
52
53 269 lower bound of the unblocking temperature spectra). However, 7 out of 12 samples show two
54
55 270 components of magnetization, with a cut-off temperature in the 540-560°C range. This suggests
56
57
58
59
60

1
2
3 271 a one-step displacement of the tektite while cooling below this temperature. This displacement
4
5 272 had to take place in a single phase and quickly (relative to the cooling time in the 585-500°C
6
7 273 range) since the two components of magnetization (MT and HT) are well-defined, precluding
8
9
10 274 progressive movement during cooling. Tektite TS6 shows a more complex demagnetization
11
12 275 with three components of magnetization unblocked over the intervals 280-520°C, 520°C-
13
14 276 575°C, and 575-580°C respectively. This suggest a more complex movement of this tektite
15
16
17 277 during cooling. When several components of magnetization are present, we consider the highest
18
19 278 temperature (and highest coercivity) component as the most representative of the original
20
21 279 position of the tektite layering, since later movements will only disturb the original orientation.
22
23
24 280 Our interpretation of the two-component magnetizations is implicitly based on the scheme of
25
26 281 two successive pTRM. A more complex possibility may be envisioned, with a part of the
27
28 282 magnetization being a chemical remanent magnetization due to the growth of magnetite grains
29
30 283 through the circa 20 nm blocking size by diffusion in the glass. But the absence of evidence for
31
32
33 284 superparamagnetic grains in the hysteresis properties (figure 3B) argues against such a scenario.
34
35
36 285

37 38 39 286 *5.4. Paleomagnetic inclination distribution*

40
41 287 The distribution of the ChRM inclination with respect to the layering plane is given in Figure 7.
42
43 288 When both thermal and AF demagnetization were available, we use the average inclination. For
44
45 289 the tektites that had two components of magnetization, we use the HC/HT component that we
46
47
48 290 consider more representative of the original tektite position, as discussed above. We included
49
50 291 the 9 inclination values obtained by de Gasparis et al. (1975), eight using AF demagnetization,
51
52
53 292 and one using thermal demagnetization. The inclination distribution is clearly different from a
54
55 293 random distribution, with a bias towards low inclinations. This is especially true if we exclude
56
57 294 the seven samples with two component of magnetization that had a more complex surface
58
59 295 history during cooling. The three samples with inclinations higher than 50° are all

1
2
3 296 multicomponent. Excluding these seven samples, the average inclination is $18 \pm 12^\circ$. (n=15,
4
5 297 including the 9 inclination values from de Gasparis et al., 1965)
6
7

8 298 This low inclination could be accounted for by a strong magnetic anisotropy of this layered
9
10 299 material, that would deviate NRM directions toward the layering plane with respect to ambient
11
12 300 field during cooling. We tested this hypothesis by measuring the anisotropy of ARM, that has
13
14 301 been shown to be a good proxy for the anisotropy of thermoremanent magnetization
15
16 302 (Gattacceca and Rochette, 2003). The anisotropy of anhysteretic remanent magnetization
17
18 303 (ARM) was approximated by assuming that the hard magnetic direction is perpendicular to the
19
20 304 layering plane. ARM was imparted in a AF field of 140 mT and a bias field 100 μ T along three
21
22 305 orthogonal direction, one of which being perpendicular to the layering plane. The minimum
23
24 306 ARM was always measured along the direction perpendicular to the layering plane. The average
25
26 307 AARM degree, computed as the maximum over the minimum ARM, is $P_{\text{ARM}} = 1.12 \pm 0.07$, with
27
28 308 a range 1.04-1.26. This would result in an average deviation of the ChRM with respect to the
29
30 309 ambient magnetic field of 2° , and a maximum deviation of 4° (considering the average
31
32 310 inclination of 18° with respect to the layering plane). This point was also discussed, with similar
33
34 311 conclusion by de Gasparis et al. (1975), using IRM anisotropy. In conclusion, magnetic
35
36 312 anisotropy cannot be responsible for the shallow inclination distribution.
37
38
39
40
41
42

43 313 As a result, the only explanation for a non random distribution of inclinations in Muong Nong
44
45 314 tektites is that the layering was sub-horizontal at the time they cooled below 585°C . The average
46
47 315 inclination of the geomagnetic field at 0.8 Ma for latitude 15°N is 28° , slightly higher than the
48
49 316 average inclination of $18 \pm 12^\circ$ measured in the Muong Nong tektites. The difference is easily
50
51 317 accounted for by the paleosecular variation of the magnetic field that can result in deviation of
52
53 318 the instantaneous geomagnetic inclination from the average inclination by as much as $15\text{-}20^\circ$
54
55 319 (e.g., Lund; 2018), as well as low data number, uncertainties on the layering plane and imperfect
56
57
58
59
60

1
2
3 320 initial horizontality of this plane. The hypothesis of a post impact cooling of Muong Nong
4
5 321 tektites with their layering horizontal on average, is thus confirmed.
6
7

8 322
9

10 323 **6. Implications for the formation of Muong Nong tektites**

11
12
13 324 The confirmation that the Muong Nong tektite layering was sub-horizontal when they cooled
14
15 325 below 585°C precludes a scenario in which layering is acquired and frozen during ejection or
16
17 326 flight (Fiske, 1996). The sub-horizontal layering is compatible with scenarii in which melt pools
18
19 327 or a melt sheet are formed either by an airburst (Wasson, 2003), or by the fallout of ejected
20
21 328 liquid material. Horizontal spreading or downslope flow in these melt pools or melt sheets
22
23 329 would have then imparted a sub-horizontal layering (e.g., Barnes and Pitakpaivan, 1962;
24
25 330 Wasson, 2003). Our results cannot discriminate between these two models (in situ melting by
26
27 331 an airburst versus fallout following an impact), although the present-day dominant model is that
28
29 332 of an impact, favored for instance by the presence of high pressure phases in Australasian
30
31 333 tektites (Cavosie et al., 2018). Moreover, the airburst model does not imply strong horizontal
32
33 334 flow and is not clearly able to produce a layering.
34
35
36
37
38

39 335 The occurrence of a few samples showing evidence of movements occurring during the cooling
40
41 336 history, when the tektite was at a temperature of 540-560°C, show that the tektite melt pools or
42
43 337 melt sheet may have behaved in a similar way as lava pool, where rotations of already solidified
44
45 338 parts are common, resulting in pahoehoe type features.
46
47
48

49 339 Although we can roughly estimate the absolute value of the inclination of the geomagnetic field
50
51 340 at the time of impact, there is no constraint about its sign. The tektite-forming impact took place
52
53 341 at 788 ± 3 ka, shortly before the Brunhes-Matuyama reversal of the geomagnetic field dated at
54
55 342 773 ka (Simon et al., 2019). The inclination of the geomagnetic field was therefore negative at
56
57 343 the location of the Muong Nong tektites. As a side result, paleomagnetism may provide a way
58
59
60

1
2
3 344 to determine the original polarity of the layering of the Muong Nong tektites, as the inclination
4
5 345 of the NRM with respect to the layering plane should be negative (i.e., the NRM should be
6
7 346 pointing up).
8
9

10 347

13 348 **7. Conclusion**

16 349 Our results show that while some Muong Nong tektites have been remagnetized by strong
17
18 350 magnetic fields, likely lightning-generated, a significant fraction retains a thermoremanent
19
20 351 magnetization acquired during cooling below 585°C in the presence of the ambient
21
22 352 geomagnetic field. This magnetization is carried by magnetite in most samples, although at
23
24 353 least one sample containing metallic iron was detected. The study of a sample with a folded
25
26 354 layering show that the folding was acquired at temperatures above 585°C. For samples with
27
28 355 simple planar layering, the inclination of the paleomagnetic direction with respect to the
29
30 356 layering plane is not random and clusters near horizontal, with an average of $18\pm 12^\circ$,
31
32 357 compatible with the inclination of the geomagnetic field for this latitude at the time of impact.
33
34 358 This confirms, based on a more extensive dataset, previous paleomagnetic results (de Gasparis
35
36 359 et al., 1975) showing that the layering of the Muong Nong tektites was sub-horizontal while
37
38 360 they were cooling below 585°C. Some tektites kept this position at least until they cooled below
39
40 361 100-200°C, while others were affected by movements suggesting a dynamic cooling
41
42 362 environment. The preferred scenario for the formation of the layering of layered tektite is
43
44 363 therefore by horizontal shear in pools or sheets of molten material. Paleomagnetism also
45
46 364 provide a way to determine the polarity of the layering of Muong Nong tektites.
47
48
49
50
51

53 365 **Acknowledgements**

56 366 This work is dedicated to the memory of John T. Wasson, for his inspiring leadership in the
57
58 367 field of meteorite and tektite studies. John suggested the topic of this article to the first author
59
60

368 during a memorable lunch in downtown Casablanca during the Meteoritical Society Meeting
 369 in 2014, and provided well-characterized samples for the study.

370

371 References

- 372 Arndt J., and Rombach N. 1976. Derivation of the thermal history of tektites and lunar glasses
 373 from their thermal expansion characteristic. *7th Lunar and Planetary Science Conference*:
 374 1123–1141.
- 375 Barnes V.E. 1963. Terrestrial implication of layering, bubble shape and minerals along faults
 376 in tektite origin. *Geochimica et Cosmochimica Acta* 28:1267–1271.
- 377 Barnes V.E. 1971. Description and origin of large tektite from Thailand. *Chemie der Erde*
 378 30:13–19.
- 379 Barnes V.E., and Pitakpaivan K. 1962. Origin of indochinite tektites. *Proceedings of the*
 380 *National Academy of Sciences* 48:947–955.
- 381 Beran, A., and Koeberl, C. 1997, Water in tektites and impact glasses by Fourier-transform
 382 infrared spectroscopy. *Meteoritics and Planetary Science* 32:211–216.
- 383 Cavosie A.J., Timms N.E., Erickson T.M., and Koeberl, C. 2018. New clues from Earth's most
 384 elusive impact crater: Evidence of reidite in Australasian tektites from Thailand. *Geology*
 385 46:203–206.
- 386 Cavosie A.J., and Koeberl C. 2019. Overestimation of threat from 100 Mt–class airbursts?
 387 High-pressure evidence from zircon in Libyan Desert Glass. *Geology* 47:1–4.
- 388 Cogné, J.P., 2003. PaleoMac: a Macintosh™ application for treating paleomagnetic data and
 389 making plate reconstructions. *Geochemistry Geophysics Geosystems* 4,
 390 <http://dx.doi.org/10.1029/2001GC000227>.
- 391 De Gasparis A.A. 1973. Magnetic properties of tektites and impact glasses. Ph.D thesis,
 392 University of Pittsburgh, 173 p.
- 393 De Gasparis A.A., Fuller M., and Cassidy W. 1975. Natural remanent magnetism of tektites of
 394 the Muong-Nong type and its bearing on models of their origin. *Geology* 3:605–607.
- 395 Di Vincenzo G., Folco L., Suttle .M.D., Brase L., Harvey R. P. 2021. Multi-collector ⁴⁰Ar/³⁹Ar
 396 dating of microtektites from microtektites from Transantarctic Mountains (Antarctica): a
 397 definitive link with the Australasian tektite/microtektite strewn field. *Geochimica et*
 398 *Cosmochimica Acta* 298:112-130.
- 399 Dunlop D. J. 2002. Theory and application of the Day plot (Mrs/Ms versus Hcr/Hc): 1.
 400 Theoretical curves and tests using titanomagnetite data. *Journal of Geophysical Research*
 401 107(B3), 2056.
- 402 Fiske P. S. 1996. Constraints on the formation of layered tektites from the excavation and
 403 analysis of layered tektites from northeast Thailand. *Meteoritics and Planetary Science*
 404 31:42–45.
- 405 Fiske P. S., Schnetzler C. C., McHone J., Chanthavaichith K. K., Homsombath I., and
 406 Phouthakayalat T. 1999. Layered tektites of Southeast Asia: Field studies in Central Laos
 407 and Vietnam. *Meteoritics and Planetary Science* 34:757–762.
- 408 Folco L., Rochette P., Perchiazzi N., D’Orazio M., Laurenzi M. A., and Tiepolo M. 2008.
 409 Microtektites from Victoria Land Transantarctic Mountains. *Geology*:36, 291–294.

- 1
2
3 410 Gattacceca J., Suavet C., Gattacceca J., and Rochette P. 2004. Toward a robust normalized
4 411 magnetic paleointensity method applied to meteorites. *Earth and Planetary Science Letters*
5 412 227:377–393.
- 6
7 413 Gattacceca J., Suavet C., Rochette P., Weiss B. P., Winklhofer M., Uehara M., and Friedrich J.
8 414 2014. Metal phases in ordinary chondrites: magnetic hysteresis properties and implications
9 415 for thermal history. *Meteoritics and Planetary Science* 49:652–676.
- 10
11 416 Glass, B.P. 1990. Tektites and microtektites: Key facts and inferences. *Tectonophysics*
12 417 171:393–404.
- 13
14 418 Glass B. P., and Barlow R. A. 1979. Mineral inclusions in Muong-Nong-type indochinites -
15 419 implications concerning parent material and process of formation. *Meteoritics* 14:55–67.
- 16
17 420 Glass B. P., and Pizzuto J. E. 1994. Geographic variation in Australasian microtektite
18 421 concentrations: Implications concerning the location and size of the source crater. *Journal*
19 422 *of Geophysical Research* 99:19,075–19,081.
- 20
21 423 Glass B. P., and Koeberl C. 2006. Australasian microtektites and associated impact ejecta in
22 424 the South China Sea and the Middle Pleistocene supereruption of Toba. *Meteoritics and*
23 425 *Planetary Science* 41:305–326.
- 24
25 426 Jourdan F., Nomade S., Wingate M., Eroglu E., and Deino A. 2019. Ultra-precise age and
26 427 temperature of formation of the Australasian tektites constrained by $^{40}\text{Ar}/^{39}\text{Ar}$ analyses.
27 428 *Meteoritics and Planetary Science* 54: 2573–2591.
- 28
29 429 Kirschvink, J.L., 1980. The least-squares line and plane and the analysis of palaeomagnetic
30 430 data. *Geophysical Journal International* 62:699–718.
- 31
32 431 Kleinmann B. 1969. Magnetite bearing spherules in tektites. *Geochimica et Cosmochimica Acta*
33 432 33:1113–1120
- 34
35 433 Koeberl C. 1992. Geochemistry and origin of Muong Nong-type tektites. *Geochimica et*
36 434 *Cosmochimica Acta* 56:1033–1064.
- 37
38 435 Koeberl C. 1994. Tektite origin by hypervelocity asteroidal or cometary impact. Target rocks,
39 436 source craters, and mechanisms, in Dressler, B.O., Grieve, R.A.F., and Sharpton, V.L.,
40 437 eds., Large Meteorite Impacts and Planetary Evolution: Geological Society of America
41 438 Special Paper 293, p. 133–152.
- 42
43 439 Krizova S., Skala R., Halodova P., Zak K., and Ackerman L. 2019. Near end-member
44 440 shenzhuangite, NiFeS₂, found in Muong Nong-type tektites from Laos. *American*
45 441 *Mineralogist* 104:1165–1172.
- 46
47 442 Lacroix, A. 1935. Les tectites sans formes figurées de l'Indochine, *Comptes-Rendus de*
48 443 *l'Académie des Sciences Paris* 200:2129–2132.
- 49
50 444 Lund S. P. 2018. A New View of Long-Term Geomagnetic Field Secular Variation. *Frontiers*
51 445 *in Earth Science*, <https://doi.org/10.3389/feart.2018.00040>
- 52
53 446 Masotta, M., Peres, S., Folco, L., Mancini, L., Rochette, P., Glass, B. P., Campanale, F.,
54 447 Gueninchault, N., Radica, F., Singsoupho, S., and Navarro, E. 2020. 3D tomographic
55 448 analysis reveals how coesite is preserved in Muong Nong-type tektites. *Scientific reports* 10,
56 449 20608. <https://doi.org/10.1038/s41598-020-76727-6>.
- 57
58 450 McElhinny M. W. 1964. Statistical significance of the fold test in palaeomagnetism.
59 451 *Geophysical Journal International* 8:338–340.
- 60
61 452 McFadden P. L., and McElhinny M. W. 1990. Classification of the reversal test in
62 453 palaeomagnetism. *Geophysical Journal International* 103:725–729.
- 63
64 454 Mizera J., Randa Z., and Kamenik J. 2016. On a possible parent crater for Australasian tektites:
65 455 Geochemical, isotopic, geographical and other constraints. *Earth-Science Reviews* 154:123–
66 456 137.

- 1
2
3 457 Mizote S., Matsumoto T., Matsuda J., and Koeberl C. 2003. Noble gases in Muong Nong-type
4 458 tektites and their implications. *Meteoritics and Planetary Science* 38:747–758.
- 5
6 459 Muxworthy A. R., Williams W. 2015. Critical single-domain grain sizes in elongated iron
7 460 particles: implications for meteoritic and lunar magnetism. *Geophysical Journal*
8 461 *International* 202:578–583.
- 9
10 462 Rochette P., Gattacceca J., Devouard B., Moustard F., Bezaeva N., Cournède C., and Scaillet
11 463 B. 2015. Magnetic properties of tektites and other related impact glasses. *Earth and*
12 464 *Planetary Science Letters* 432:381–390.
- 13 465 Rochette P., Bezaeva N., Kosterov A., Gattacceca J., Masaitis V., Badyukov D. Giuli G.,
14 466 Lepore G.O., Beck P. 2019. Magnetic Properties and Redox State of Impact Glasses: A
15 467 Review and New Case Studies from Siberia. *Geosciences* 9 (5), 225
- 16
17 468 Rochette, P., Beck, P., Braucher, R., Cornec, J., Debaille, V., Devouard, B., Gattacceca, J.,
18 469 Jourdan, F., Moustard, F., Moynier, F., Nomade, S., and Reynard, B. 2021. A new tektite
19 470 strewn-field and source crater couple discovered in Central America: insights into the
20 471 tektite generation process and its ubiquity. *Communications Earth & Environment*, in
21 472 press.
- 22
23 473 Schnetzler C. C. 1992. Mechanism of Muong Nong-type tektite formation and speculation on
24 474 the source of Australasian tektites. *Meteoritics* 27:154–165.
- 25 475 Schnetzler C. C., and McHone J. F. 1996. Source of Australasian tektites: Investigating
26 476 possible impact sites in Laos. *Meteoritics and Planetary Science* 31:73–76.
- 27
28 477 Sieh K., Herrin J., Jicha B., Schonwalder Angel D., James S., Moore D.P., Banerjee
29 478 P., Wiwegwin W., Sihavong V., Singer B., Chualaowanich T., and Charusiri P. 2020.
30 479 Australasian impact crater buried under the Bolaven volcanic field, Southern Laos.
31 480 *Proceedings of the National Academy of Sciences* 117:1346–1353.
- 32
33 481 Simon Q., Sukanuma Y., Okadad M., Hanedad Y., and ASTER Team. 2019. High-resolution
34 482 ¹⁰Be and paleomagnetic recording of the last polarity reversal in the Chiba composite
35 483 section: Age and dynamics of the Matuyama–Brunhes transition. *Earth and Planetary*
36 484 *Science Letters* 519:92–100.
- 37
38 485 Tada T., Tada R., Chansom P., SONGtham W., Carling P.A., and Tajika E. 2020. In situ
39 486 occurrence of Muong Nong-type Australasian tektite fragments from the Quaternary
40 487 deposits near Huai Om, northeastern Thailand. *Progress in Earth and Planetary Science*
41 488 66,7.
- 42
43 489 Verrier V., and Rochette P. 2002. Estimating peak currents at ground lightning impacts using
44 490 remanent magnetization. *Geophysical Research Letters* 29(18), 1867.
- 45 491 Wasson J. T. 1991. Layered tektites: a multiple impact origin for the Australasian tektites. *Earth*
46 492 *and Planetary Science Letters* 102:95–109.
- 47
48 493 Wasson J. T., Pitakpaivan K., Putthapiban P., Salyapongse S., Thapthimthong B., and McHone
49 494 J. F. 1995. Field recovery of layered tektites in Northeast Thailand. *Journal of Geophysical*
50 495 *Research-Planets* 100:14383–14389.
- 51 496 Wasson J. T. 2003. Large aerial bursts: an important class of terrestrial accretionary events.
52 497 *Astrobiology* 3:163–79
- 53
54 498 Wilding M., Webb S., and Dingwell D. B. 1996. Tektite cooling rates: Calorimetric relaxation
55 499 geospeedometry applied to a natural glass. *Geochimica et Cosmochimica Acta* 60:1099–
56 500 1103.
- 57
58 501 Žák K., Skala R., Randa Z., and Mizera J. 2019. A review of volatile compounds in tektites,
59 502 and carbon content and isotopic composition of moldavite glass. *Meteoritics and Planetary*
60 503 *Science* 47:1010–1028.

504

505 **Captions**

506 **Figure 1.** Location of studied samples. The coordinates for samples studied in de Gasparis et
507 al. (1973) are from de Gasparis (1971).

508 **Figure 2.** Pictures of a selection of studied tektites, before cutting to extract a sample oriented
509 with respect to the layering. For each sample, a picture of a thin slice in transmitted light is
510 shown to highlight the layering.

511 **Figure 3.** A) Mass-normalized hysteresis cycles for Muong Nong tektites samples N20A and
512 T428, corrected for the paramagnetic and diamagnetic contribution computed over the 0.8-1 T
513 interval. B) Hysteresis parameters for all measurable samples. Horizontal and vertical lines
514 roughly divide the plot into regions with single domain (SD), pseudo-single domain (PSD),
515 superparamagnetic (SP) and multidomain (MD) behavior. The gray curves represent mixtures
516 of PSD, SD, and MD grains for magnetite (from *Dunlop, 2002*)

517 **Figure 4.** A) Evolution of NRM during thermal demagnetization. Sample T420 that was
518 demagnetized by a combination of AF and thermal demagnetization is not shown. Sample T490
519 that contains metallic iron is indicated. B) Evolution of sIRM during AF demagnetization. The
520 five samples with highest coercivity are indicated. C) Evolution of NRM during AF
521 demagnetization. Samples that were remagnetized by lightning are not shown in figures A and
522 C.

523 **Figure 5.** REM' versus AF field for representative samples: magnetized by strong field (N3A),
524 partially magnetized by strong field (MNP1), devoid of strong field magnetization (T490).
525 REM' is the equal to $\Delta\text{NRM}/\Delta\text{IRM}$ over successive AF demagnetization steps (see Gattacceca
526 and Rochette, 2004 for lengthy explanations).

1
2
3 527 **Figure 6.** Orthogonal plot of demagnetization data for all studied samples not remagnetized by
4
5 528 lightning. Among samples remagnetized only lightning, only N17 is shown for example. The
6
7 529 demagnetization data are projected on two orthogonal planes: layering plane (solid symbols),
8
9 530 and a plane orthogonal to the layering (open symbols). Boxes indicate sub samples from the
10
11 531 same tektite. The AF or temperature is indicated from some steps.

12
13
14
15 532 **Figure 7.** Histogram of inclinations of the characteristic remanent magnetization with respect
16
17 533 to layering. Samples from this study with a single component of magnetization are highlighted,
18
19 534 followed by data from de Gasparis et al. (1975), followed by samples with two components of
20
21 535 magnetization (MT/MC and HC/HT). Distribution for an equivalent number of random
22
23 536 directions is shown (N=21 for all data, N=14 without the multicomponent samples, N=5 with
24
25 537 our single component samples only).
26
27
28
29
30
31
32
33
34
35
36
37
38
39
40
41
42
43
44
45
46
47
48
49
50
51
52
53
54
55
56
57
58
59
60

1
2
3
4
5 Jérôme Gattacceca
6 e-mail:gattacceca@cerege.fr
7
8
9
10

11 Editor of *MAPS*

12
13
14 Aix-en-Provence, April 19, 2021
15
16
17
18
19

20 Dear Editor,
21

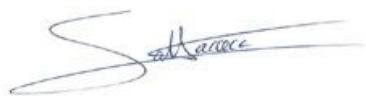
22
23 Please find attached a manuscript called "*Revisiting the paleomagnetism of Muong Nong layered*
24 *tektites: implications for their formation process*" by myself and co-authors that we would like to
25 submit to *Meteoritics and Planetary Sciences* for the special issue honoring John Wasson.
26

27
28 Indeed, the topic of this study was suggested to us in 2014 by John Wasson who had a long time
29 interest in tektites and in Muong Nong tektites in particular. He also selected the samples for the study.
30 Unfortunately, I was not able to complete the study before he passed away.
31

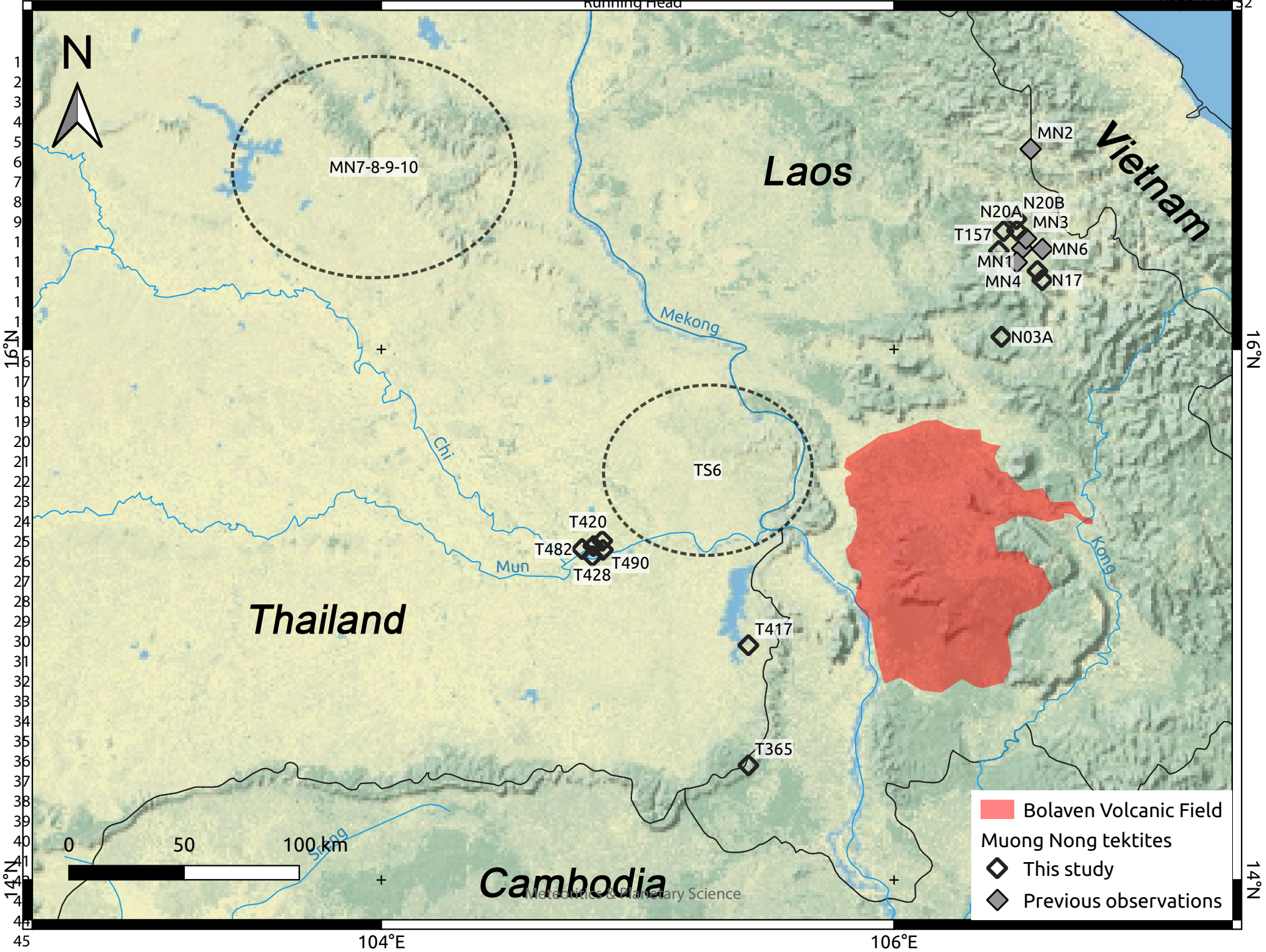
32
33 The original scope of this paleomagnetic study was to confirm that the layering of Muong Nong
34 tektites was sub-horizontal at the time these glasses were cooling. In addition to this confirmation, that
35 provide constraints on the formation mechanism of these tektites, we provide interesting data about
36 the magnetic mineralogy of this unusual material.
37

38 Yours sincerely,
39
40
41

42
43
44
45
46



47 Jérôme Gattacceca
48
49
50
51
52
53
54
55
56
57
58
59
60



N

MN7-8-9-10

Laos

Vietnam

Mekong

Chi

TS6

Mun

T420

T482

T428

T490

T417

T365

Kong

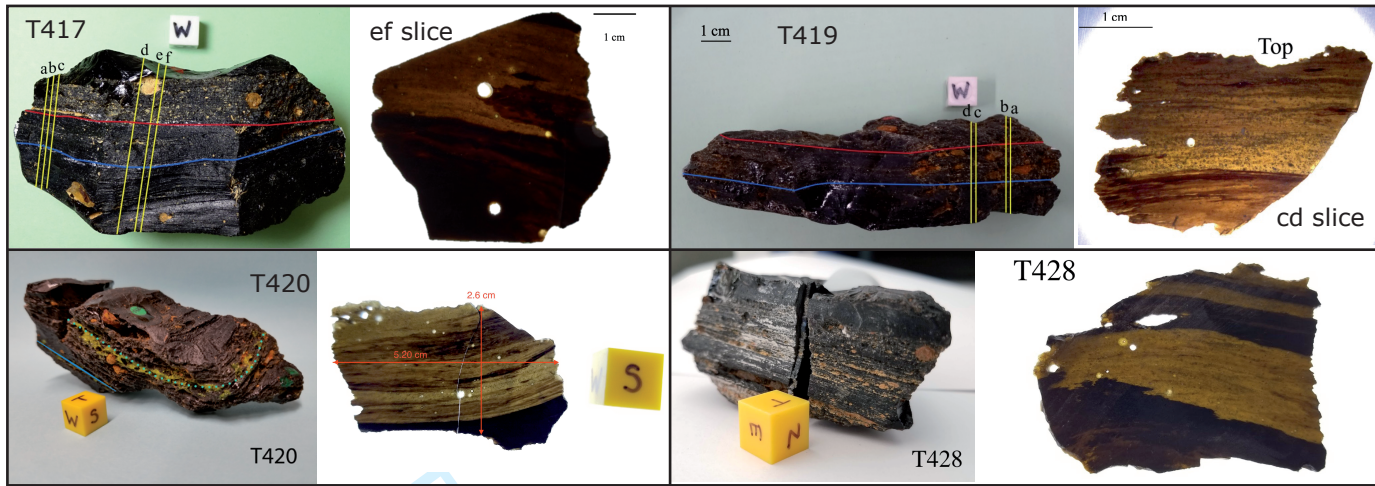
Thailand

Cambodia

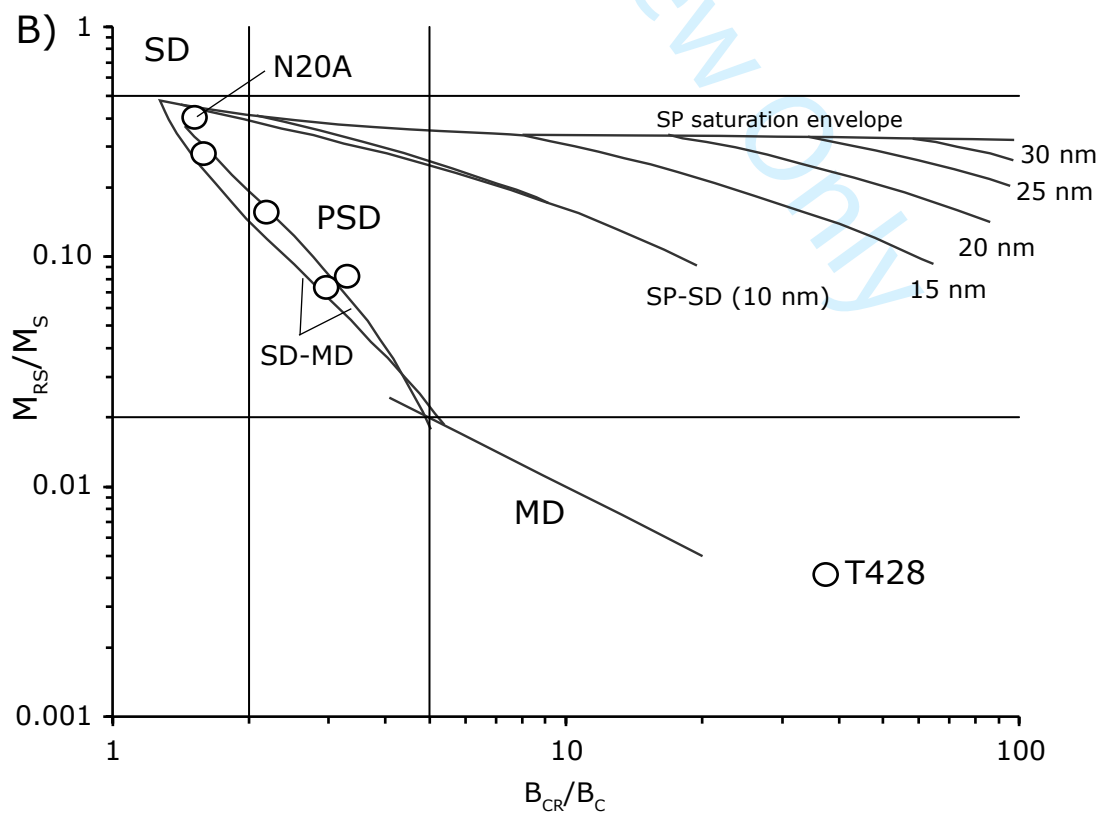
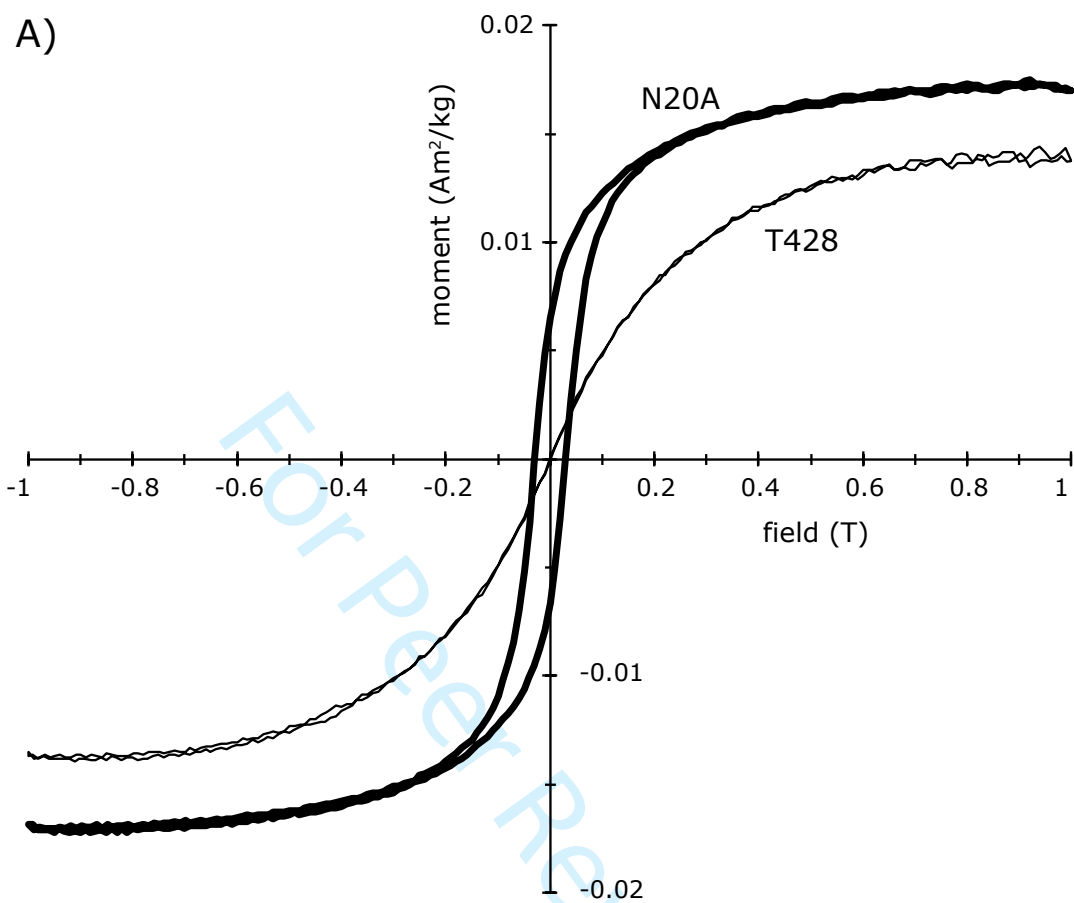
- Bolaven Volcanic Field
- Muong Nong tectites
- This study
- Previous observations

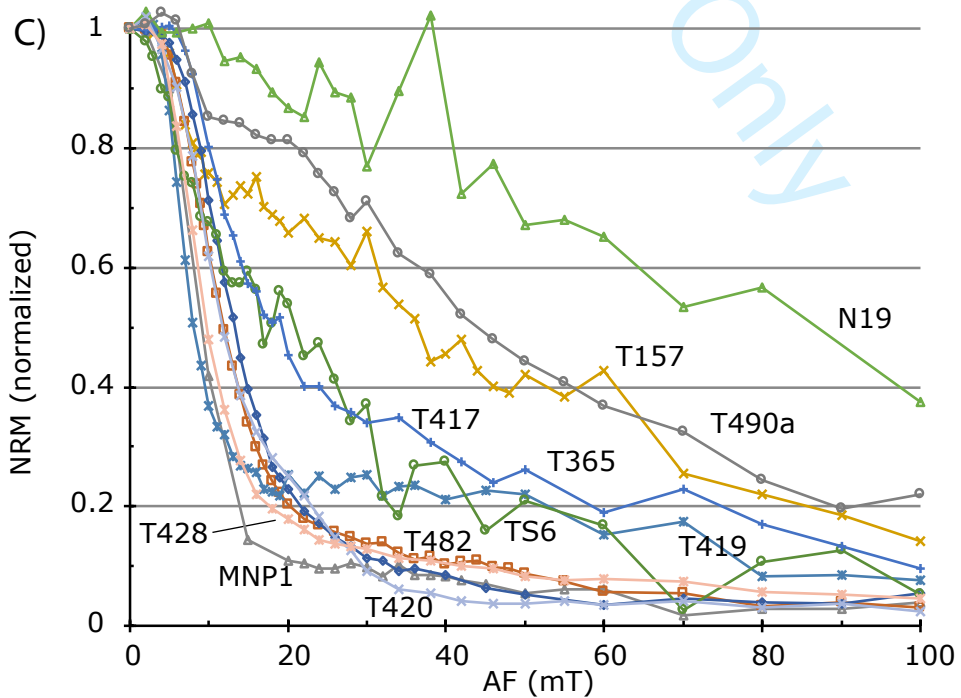
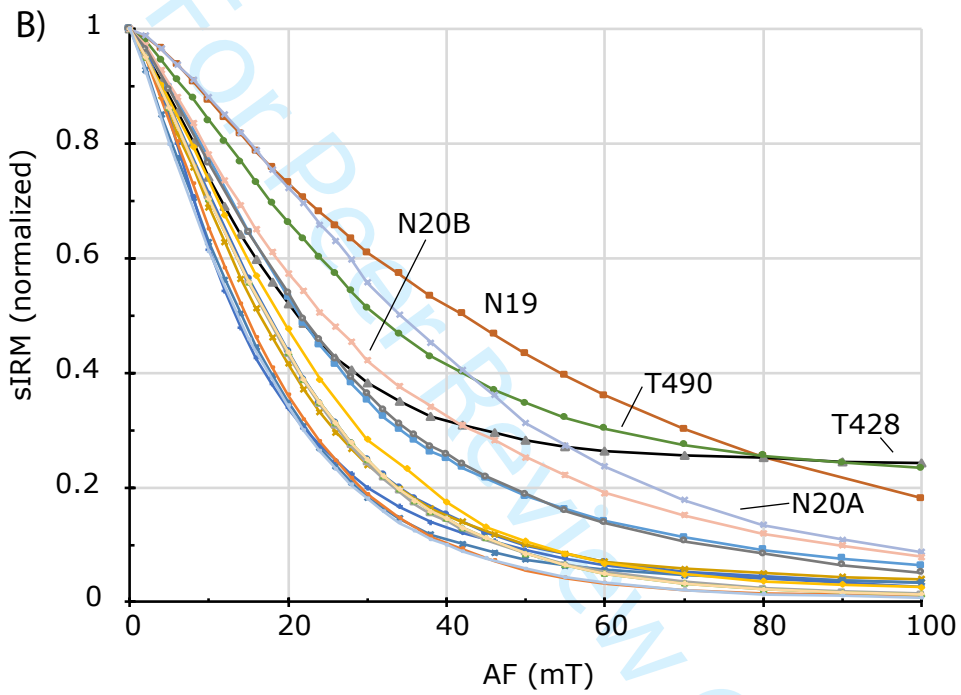
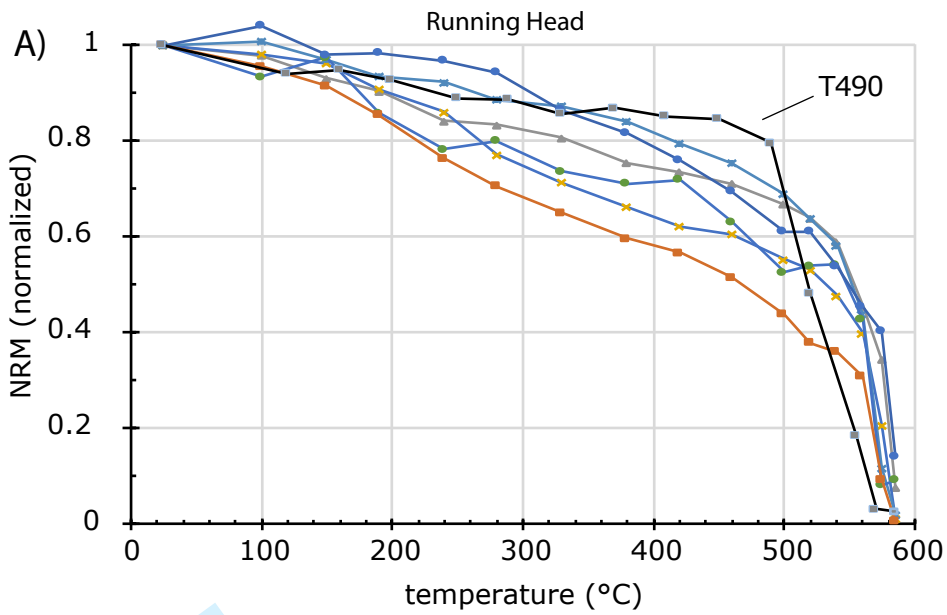
0 50 100 km

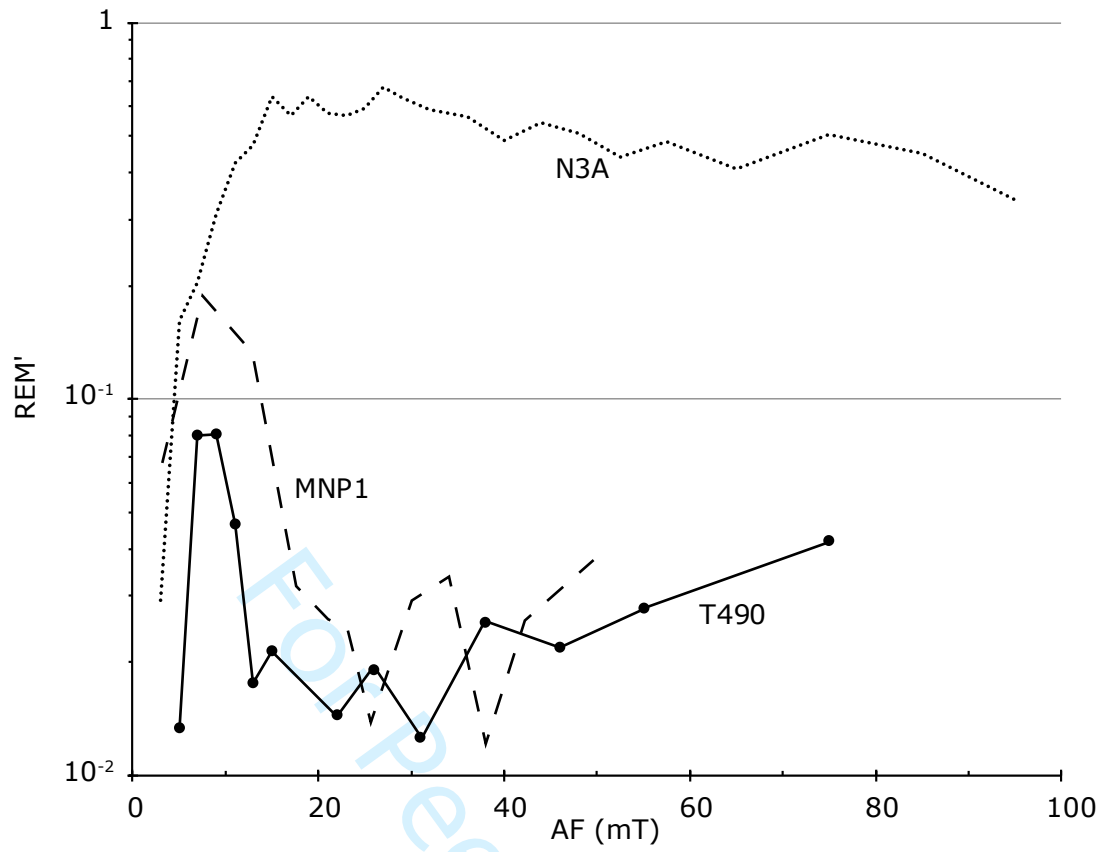
1
2
3
4
5
6
7
8
9
10
11
12
13
14
15
16
17
18
19
20
21
22
23
24
25
26
27
28
29
30
31
32
33
34
35
36
37
38
39
40
41
42
43
44
45
46
47
48
49
50
51
52
53
54
55
56
57
58
59
60



For Peer Review Only

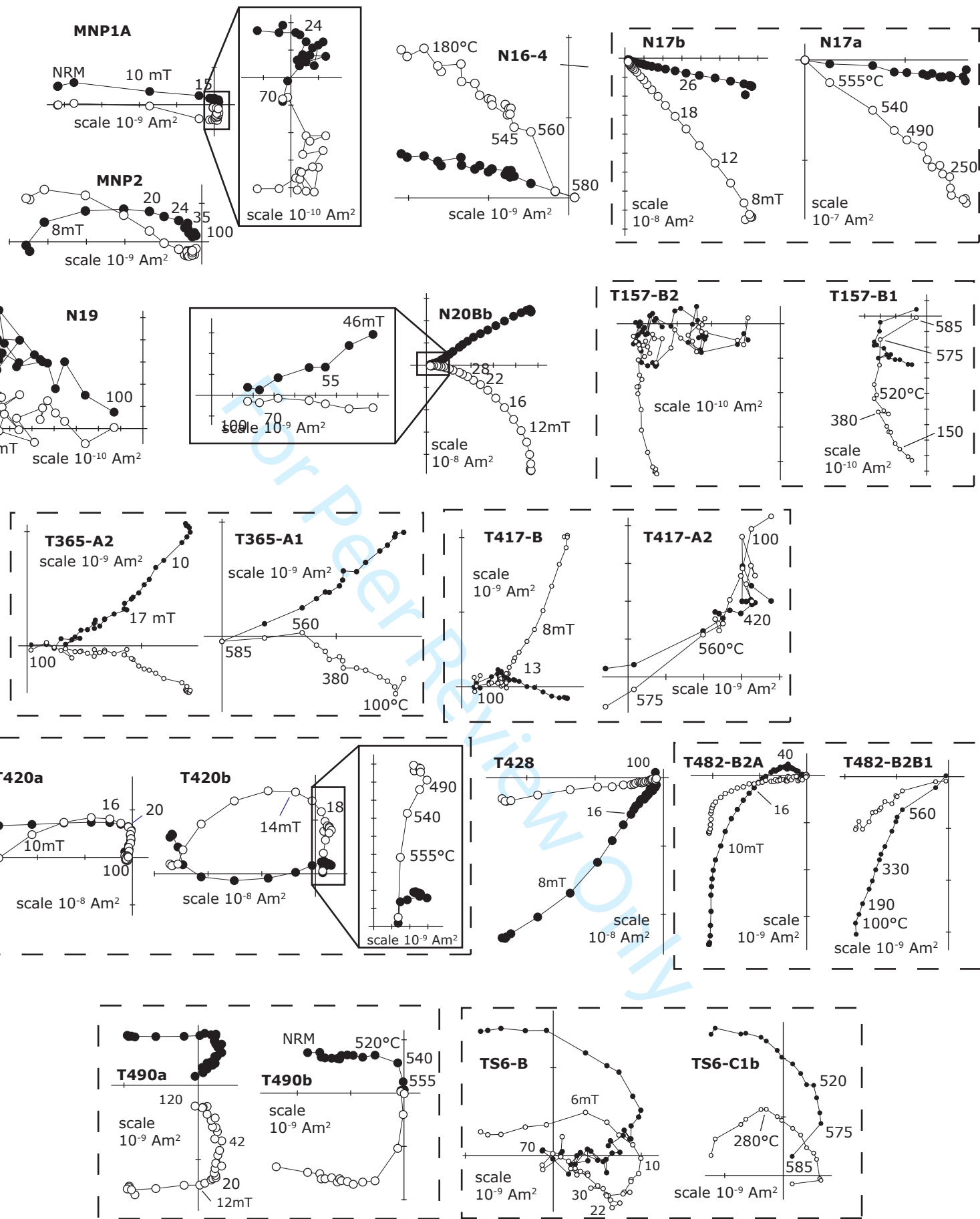


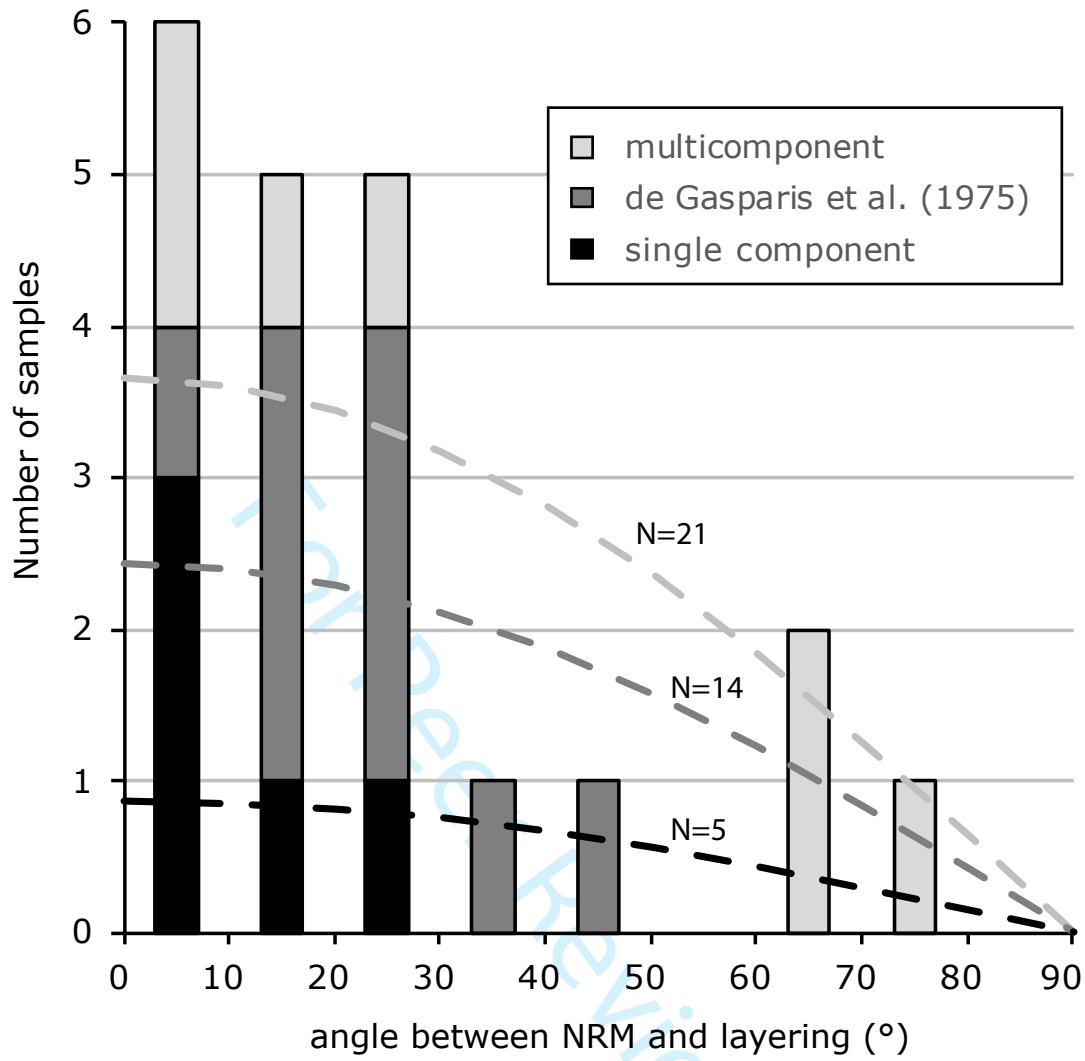




1
2
3
4
5
6
7
8
9
10
11
12
13
14
15
16
17
18
19
20
21
22
23
24
25
26
27
28
29
30
31
32
33
34
35
36
37
38
39
40
41
42
43
44
45
46
47
48
49
50
51
52
53
54
55
56
57
58
59
60

1
2
3
4
5
6
7
8
9
10
11
12
13
14
15
16
17
18
19
20
21
22
23
24
25
26
27
28
29
30
31
32
33
34
35
36
37
38
39
40
41
42
43
44
45
46
47
48
49
50
51
52
53
54
55
56
57
58
59
60





1 **Tables**2 **Table 1: List of studied samples.**

sample	mass (g)	latitude N	longitude E	area	collection
MNP1	95			Thailand (?)	CEREGE collection£
MNP2	350			Thailand (?)	CEREGE collection£
N03A	278	16°02'48.72"	106°25'08"	Muong Nong area, Southern Laos	CEREGE collection\$
N03B	128	16°02'48.72"	106°25'08"	Muong Nong area, Southern Laos	CEREGE collection\$
N16	210	16°17'37.5"	106°33'33.2"	Muong Nong area, Southern Laos	CEREGE collection\$
N17	275	16°15'33.5"	106°34'40.4"	Muong Nong area, Southern Laos	CEREGE collection\$
N19	36	16°26'32"	106°28'06.3"	Muong Nong area, Southern Laos	CEREGE collection*
N20A	49	16°26'34.5"	106°28'48.7"	Muong Nong area, Southern Laos	CEREGE collection*
N20B	36	16°26'34.5"	106°28'48.7"	Muong Nong area, Southern Laos	CEREGE collection*
TS6	6000			SE of Ubon Ratchathani, Thailand	Smithsonian Institution
T157	179	~16°22'	~106°30'	Muong Nong area, Southern Laos	UCLA collection
T365	322	14°26'0"	105°25'54"	Ban Nong Paen, North East Thailand	UCLA collection
T417	288	14°53'12"	105°25'54"	Ban Huai Sai, North East Thailand	UCLA collection
T419	215	~14°54'	~105°25'	Ban Huai Sai, North East Thailand	UCLA collection
T420	348	~14°54'	~105°25'	Ban Huai Sai, North East Thailand	UCLA collection
T428	127	~14°54'	~105°25'	Ban Huai Sai, North East Thailand	UCLA collection
T482	546	~14°54'	~105°25'	Ban Huai Sai, North East Thailand	UCLA collection
T490	183	~14°54'	~105°25'	Ban Huai Sai, North East Thailand	UCLA collection

3

4 *collected in situ, \$: bought from villagers, £: bought from a dealer

5

6

7 Table 2: **Hysteresis properties**

sample	mass (g)	M_S ($10^{-3} \text{ Am}^2/\text{kg}$)	M_{RS} ($10^{-3} \text{ Am}^2/\text{kg}$)	B_C (mT)	B_{CR} (mT)	χ_{HF} ($10^{-9} \text{ m}^3/\text{kg}$)	χ ($10^{-9} \text{ m}^3/\text{kg}$)
N17	0.23	8.3	2.24	27	43	60.1	133
N20A	1.04	16.6	6.47	29.4	45.1	61.1	205
N20B	5.14	0.8	0.120	16	35	54.4	147
T419	0.74	1	0.080	9	30	81.9	108
T428	1.22	13.1	0.052	0.8	30	54.8	133
TS6	1.92	1.5	0.105	9	27	65.1	106

8

9 M_S : saturation magnetization, M_{RS} : saturation remanence, B_C : coercivity, B_{CR} : coercivity of remanence, χ_{HF} : high-field (paramagnetic +
10 diamagnetic) susceptibility, χ : low-field susceptibility.

11

12 **Table 3. Paleomagnetic results**

sample	sub-sample	method	mass (g)	NRM (Am ² /kg)	sIRM (Am ² /kg)	MDF ARM (mT)	MDF sIRM (mT)	χ (10 ⁻⁹ m ³ /kg)	HC/HT component			MC/MT component				
									range	n	I (°)	MAD (°)	range	n	I (°)	MAD (°)
MNP1		AF	1.81	2.33×10 ⁻⁶	3.87×10 ⁻⁵	28	17	81.9	24-70 mT	15	73.2	29.3	5-20 mT	4	-7.2	3
MNP2		AF	16.1	2.87×10 ⁻⁷	1.12×10 ⁻⁵	32	19	99.3	16-70 mT	12	-28	9.3				
N03A [†]	a	AF	9.83	6.52×10 ⁻⁶	1.62×10 ⁻⁵	30	16.5	77.3								
N03B [†]	a	Th	10.69	3.34×10 ⁻⁶				80.5	330-585 mT	10	51.9	2.6				
N03B [†]	b	AF	4.65	5.16×10 ⁻⁶	2.17×10 ⁻⁵	13	13	80.5	14-100 mT	19	45.4	1.3				
N16	1	Th	17.9	1.49×10 ⁻⁷				93.6								
N16	2	Th	14.71	5.14×10 ⁻⁸				87.3								
N16	3	Th	14.86	6.93×10 ⁻⁸				86.9								
N16	4	Th	11.58	2.46×10 ⁻⁷				87.7								
N17 [†]	a	Th	10.75	1.97×10 ⁻⁵				83.5	250-585°C	12	38.6	2.6				
N17 [†]	b	AF	5.85	1.85×10 ⁻⁵	1.28×10 ⁻⁴	24	15	83.5	10-80mT	20	48.8	0.9				
N19		AF	10.47	7.01×10 ⁻⁸	8.26×10 ⁻⁶	26	42	88.6	4-120 mT	23	16.9	21.3				
N20A [†]	a	AF	6.98	5.79×10 ⁻⁴	1.91×10 ⁻³	40	34	147.3	8-70 mT	20	15.6	1.4				
N20A [†]	b	Th	6.14	9.27×10 ⁻⁴				147.3	100-585 °C	16	15.1	1.1				
N20B	b	AF	5.15	1.37×10 ⁻⁵	1.20×10 ⁻⁴	43	24	86.6	46-100 mT	7	3.3	5.5				
T157	B1	Th	5.89	1.68×10 ⁻⁷				80.6	575-585 °C	2	26	8.9	540-575	3	65.6	4.3
T157	B2	AF	2.84	2.03×10 ⁻⁷	1.41×10 ⁻⁴	32	21	81.3	13-90 mT	27	9.5	21.7	5-12 mT	10	65.9	9.1
T365	A1	Th	0.44	4.24×10 ⁻⁶				83.4	560-585 °C	4	-4.5	2.9	100-560 °C	15	23.5	5.5
T365	A2	AF	0.40	4.46×10 ⁻⁶	7.61×10 ⁻⁵	30	22	84.5	20-100 mT	16	5	10.7	8-17 mT	9	18.6	4.9
T417	A2	Th	2.90	2.08×10 ⁻⁷				89.9	540-580 °C	4	-32.6	2.9	240-540 °C	10	-58.2	19.8
T417	B2	AF	3.26	7.48×10 ⁻⁷	3.50×10 ⁻⁵	29	17	88.1	15-100 mT	22	-7.3	7.5	5-15 mT	11	-61.9	3.3
T419 [†]	B3b	Th	0.40	5.29×10 ⁻⁶				108.3	500-585 °C	6	57.7	3.2				
T419 [†]	B2	AF	0.74	6.97×10 ⁻⁶	7.23×10 ⁻⁵	28	17	96.6	12-100 mT	25	58.6	3.1				
T420	a	AF	11.12	3.29×10 ⁻⁶	8.05×10 ⁻⁵	31	14	94.8	22-120 mT	18	-46.4	6.3	8-20 mT	6	5.1	8.4
T420	b	Th ^e	14.26	1.96×10 ⁻⁶				96.1	250-570 °C ^a	11	-76.7	6.3				
T428		AF	13.33	2.51×10 ⁻⁶	5.59×10 ⁻⁵	50	21	132.7	22-100 mT	18	8.5	7.3				
T482	B2B1	Th	1.11	3.29×10 ⁻⁶				94.6	100-585°C	18	15.7	8				
T482	B2A	AF	1.55	2.80×10 ⁻⁶	5.23×10 ⁻⁵	28	17	93.5	34-90 mT	15	2.2	19.7				
T490	a	AF	14.41	1.26×10 ⁻⁷	8.54×10 ⁻⁶	38	31	84.9	18-120 mT	20	64.4	9.6	2-14 mT	7	3.6	2.4
T490	b	Th	16.63	1.84×10 ⁻⁷				81.2	540-585 °C	4	63.6	4.1	25-520 °C	12	-8	9
TS6	C1b	Th	1.96	1.39×10 ⁻⁶				103.1	560-585 °C	4	-5.3	6.1	280-560 °C	10	-37.5	7.6
TS6	B	AF	1.90	8.74×10 ⁻⁷	1.16×10 ⁻⁴	18	13	106.5	22-100 mT	17	32.5	20.6	9-20 mT	11	-44.6	17

13

1
2
3 14 †: remagnetized by lightning; £: demagnetized by AF to 18 mT before thermal demagnetization. MDF: median destructive field, I: angle between
4
5 15 the magnetization component and the layering plane, MAD: maximum angular deviation, n: numbers of steps used in the computation of the
6
7
8 16 magnetization component.
9
10
11
12
13
14
15
16
17
18
19
20
21
22
23
24
25
26
27
28
29
30
31
32
33
34
35
36
37
38
39
40
41
42
43
44
45
46

For Peer Review Only